On the three-dimensionality of shock-wave / laminar boundary layer interaction

Jean-Christophe ROBINET

SINUMEF Lab. ENSAM Paris, 151 boulevard de l'Hôpital, 75013 Paris.
jean-christophe.robinet@paris.ensam.fr

Abstract. Three-dimensional direct numerical simulation (DNS) of shock-wave / laminar boundary layer interaction (SWLBLI) is performed with for objective to show that a SWLBLI can exhibit self-sustained low frequency oscillations and a three-dimensional flow when the interaction is high. A linearized global stability analysis is carried out in order to find some characteristics observed in the DNS. This stability analysis permits to show that the physical origin to the three-dimensionality of the flow results from the existence of a three-dimensional stationary global instability.

Key words: global instability, DNS, shock-wave / laminar boundary-layer interaction.

1. Introduction

The principal objective of this paper is to study some unsteady characteristics of an interaction between an incident oblique shock wave impinging on a laminar boundary layer developing on a flat plate. More precisely, this paper shows that some unsteadiness, in particular the low frequency unsteadiness, originate in a supercritical Hopf bifurcation related to the dynamics of the separated boundary layer. Various direct numerical simulations were carried out of a shock-wave/laminar boundary-layer interaction, resulting from the test case studied by Degrez *et al.* (1987). Three-dimensional unsteady Navier-Stokes equations are numerically solved with an implicit dual time stepping for the temporal algorithm and high order AUSMPW+ scheme for the spatial discretization. A parametric study on the oblique shock-wave angle has been performed to characterize the unsteady behaviour onset. These numerical simulations have shown that starting from the incident shock angle and the spanwise extension, the flow becomes three-dimensional and unsteady. A linearized global stability analysis is carried out in order to specify and to find some characteristics observed in the direct numerical simulation. This stability analysis permits to show that the physical origin generating the three-dimensional characters of the flow results from the existence of a three-dimensional stationary global instability.

2. Physical Configurations

In the following, only shock wave / laminar boundary layer interaction on flate-plate has been investigated. The test case considered has been experimentally and numerically studied by Degrez *et al.* [2]. The free-stream inflow Mach number is 2.15 for the numerical simulation. The Reynolds number based on the distance X_{sh} between the plate leading edge and the shock impingement point is 10^5. The shock angle with respect to the horizontal is equal to $\theta = 30.8^o$, which corresponds to a shock generator angle of 3.75^o. This dataset takes into account confinement, 3D effects and measurement approximations; it

Parameter	**Value**
Freestream Mach number	$M_\infty = 2.15$
Interaction length	$X_{sh} = 8 \times 10^{-2}$ m
Freestream Reynolds number	Re=10^5
Incident shock angle	$\theta = [30.8^o; 33^o]$
Spanwise length	$L_z = [0.1; 3]$
Prandtl number	Pr=0.72
Ratio of specific heats	$\gamma = 1.4$

Table 1. Flow parameters for the SWBLI.

is not strictly the same as the experimental free-stream conditions (see [2] for more details). At this incidence angle, Degrez *et al.* indicate that the flow remains stationary and two-dimensional upstream, downstream and in the interaction. Furthermore it remains laminar at least until the end of the measurement zone. Table 1 gives the different physical parameters.

To demonstrate that the low frequency behaviour observed in some SWBLI configurations can be linked to the intrinsic dynamics of the detached zone induced by the interaction, independently of the turbulent boundary layer characteristics, the evolution of an incident shock wave impinging a laminar boundary layer developing over a flat plate when the incident shock angle is gradually increased. The free-stream inflow Mach number and the global Reynolds number remain unchanged. The evolution of the SWBLI when the incident shock angle increases is a very complex problem. Indeed, for a particular value of the angle θ, the flow becomes transitional in the interaction zone. This transitional state will probably modify substantially the topology and the dynamics of the interaction zone. In addition, no unsteady disturbance, of convective instability type, is introduced at the upstream end of the computational domain in order not to start possible instabilities of convective nature which could mask and/or modify the existence of a global instability. Three-dimensional numerical simulations will be carried out without taking into account the transitional character of SWBLI. Considering these assumptions, these present computations are meant to show that a SWBLI can become unsteady without taking into account the turbulent character of the flow. In this scenario, the unsteadiness onset is directly linked to the intrinsic dynamics of the detached zone and quickly leads toward a three-dimensional and unsteady flow.

3. Computational Domain and Boundary Conditions

The coordinates are non-dimensionalized by the interaction length X_{sh}. The geometry of the 3D domain is $\mathcal{D} = [0.2; 2.3] \times [0; 0.94] \times [0, L_z]$ with $600 \times 180 \times 60$ points. The grid is uniform in the streamwise and spanwise directions and geometrical in the normal direction. The transverse direction L_z lies between 0.1 and 3 with a number of planes ranging between 40 and 60 planes. The 3D dimensionless mesh spacing is equal to $\Delta x = 3 \times 10^{-3}$, $\Delta y = 7.8 \times 10^{-5}$ at the wall and from $\Delta z = 1.05 \times 10^{-3}$ to $\Delta z = 1.66 \times 10^{-2}$. The whole of the numerical parameters necessary to the numerical simulation is gathered in table 2.

The steady two-dimensional Navier-Stokes solution is imposed at the inflow ($x = 0.2$).

Parameter	**Value**
(N_x, N_y, N_z)	$(600, 180, 60)$
$(\Delta x, (\Delta y)^{wall}, \Delta z)$	$(3 \times 10^{-3},\ 7.8 \times 10^{-5},\ 1.66 \times 10^{-2})$
Geometrical ratio q	$q = 1.02$
$x_{in}, x_{sponge}, x_{out}$	$0.2,\ 2,\ 2.3$
$y \in [0, y_{max}]$	$y \in [0; 0.94]$
$z \in [0, L_z]$	$z \in [0; 1]$
dual CFL	50
physical CFL	6
time step	6.82×10^{-6}

Table 2. Computational parameters for the SWBLI.

This latter is repeated in the spanwise direction. The inflow boundary condition is thus homogeneous according to z. At the outflow and at the upper boundary, extrapolations are used as boundary conditions for the conservative variables. The flat-plate is assumed to be an adiabatic wall where the velocity vector is zero (no-slip condition); pressure is also extrapolated from the values just above the plate. A sponge zone is imposed from $x = 2$ to $x = 2.3$. At the wall, the simulation uses viscous conditions for the velocities and a constant temperature condition, and it computes density from the continuity equation. In spanwise direction, the solution can be characterized as a neutral oscillation, which is periodic at its boundaries. These boundary conditions are classically used in direct numerical simulation but will have important consequences on the results analyzed in this study. Indeed, in the case of a flow that naturally produces 3D structures, the dimension L_z given to the domain in the z-direction will force the wavelength of the spanwise structures. Therefore, the spanwise dimension should ideally be as large as possible to let 3D instabilities appear spontaneously. The present SWBLI study is focused on low frequency phenomena with corresponding large wavelengths. It was therefore decided to consider L_z as a parameter rather than a fixed input data; for all the 3D computations a parametric study on L_z is needed. The computational parameters are reported in table 2.

4. Direct Numerical Simulations

4.1. Numerical Method

The governing equations are solved using a fifth-order-accurate AUSMPW+ scheme for space discretization initially developed by [3]. High-accuracy of the inviscid numerical fluxes is ensured through the use of a fifth-order MUSCL reconstruction of the primitive variables vector $(\rho, u, v, w, p)^t$. No limiter is used to cross the shock. A time-accurate approximate solution of governing equations is obtained using the following implicit second-order linear multi-step method. In order to efficiently solve the implicit system, we make use of a dual time technique.

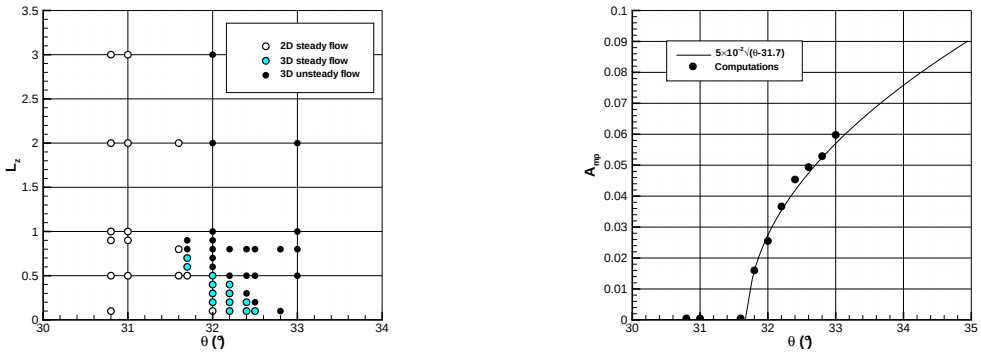

Figure 1. Left: flow organization according to θ and L_z., right: the amplitude of the oscillations of w as a function of θ. • : Numerical simulations, line : $A_w \sim \sqrt{\theta - 31.7}$ for $L_z = 0.8$.

4.2. DIRECT NUMERICAL SIMULATIONS RESULTS

Many computations were carried out for various values of the incident shock angle $\theta \in [30.8^o; 34^o]$ and spanwise length $L_z \in [0.1; 3]$. In agreement with the experimental results of Degrez, for $\theta = 30.8^o$ and all L_z, the solution obtained is two-dimensional and steady. When the incident shock angle is greater, for the same flow conditions (Re, M), the flow is destabilized towards a complex space-time dynamical state. When $31.7^o < \theta < 32.8^o$, the two-dimensional flow is conditionally stable with respect to the spanwise length L_z. Indeed, there are two critical spanwise lengths, $L_{z_{c_1}}(\theta)$ and $L_{z_{c_2}}(\theta)$, where the flow bifurcates. If $L_{z_{c_1}}(\theta) < L_z < L_{z_{c_2}}(\theta)$, the SWBLI bifurcates towards a three-dimensional and stationary asymptotic state. If $L_z > L_{z_{c_2}}(\theta)$, the asymptotic state corresponds to a three-dimensional and unsteady flow. When $\theta > 32.7^o$, a three-dimensional and unsteady flow is directly reached. Fig. 1-left synthesizes the results obtained. In order to characterize this bifurcation, an amplitude parameter is defined as $A_w = \max(w(t)) - \min(w(t))$, where max $(w(t))$ and min $(w(t))$ are the maximum and the minimum of the spanwise velocity component, $w(t)$, respectively. Figure 1-right shows the amplitude of the oscillations of w in a particular point in the SWBLI for the established flow and for $L_z = 0.8$. As shows in figures 2 (a)-(d), when the incident shock angle increases, the SWBLI becomes gradually three-dimensional. This three-dimensionality, for all the configurations studied in this paper, remains confined in the interaction zone and more precisely in the separated zone. Figure 3 presents, in given point $(x_0, y_0, z_0) = (1.1, 2 \times 10^{-2}, 0.4)$ the time flow evolution of the spanwise velocity component in log scale. This run has been initialized by two-dimensional solution. After a short transient state (before point B), the amplitude of spanwise velocity component increases exponentially (linear evolution). When this amplitude reaches a finite amplitude a nonlinear saturation takes place (point C). From point C to point E, the spanwise velocity amplitude remains constant. When $t > 60$ ms, the Hopf bifurcation, previously described appears. This characteristic is observed in all flow cases. The linear amplification rate observed in stage (B-C) is similar in any point of the flow. These results suggest the existence of global instability mechanism. In next the section, this characteristic will be demonstrated.

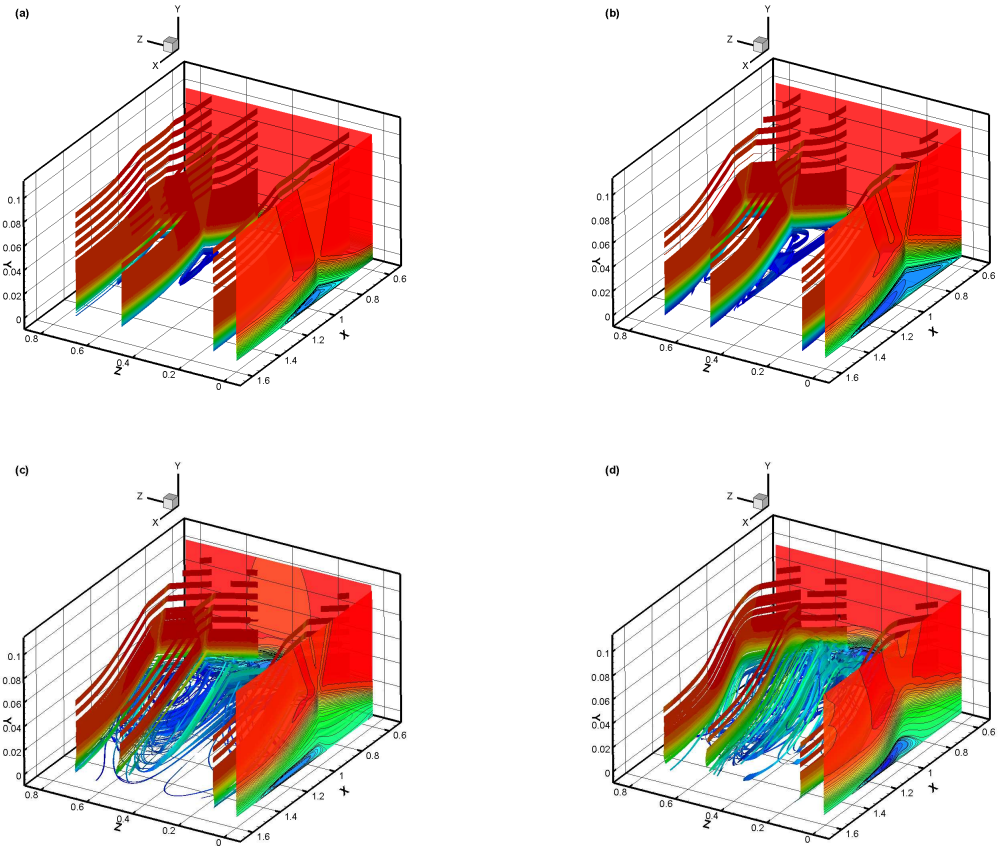

Figure 2. Iso-lines of longitudinal velocity $\overline{U}(x, y)$ and streamlines for $L_z = 0.8$. (a): $\theta = 30.8^o$, (b): $\theta = 31.7^o$, (c):$\theta = 32.0^o$ and (d): $\theta = 32.5^o$.

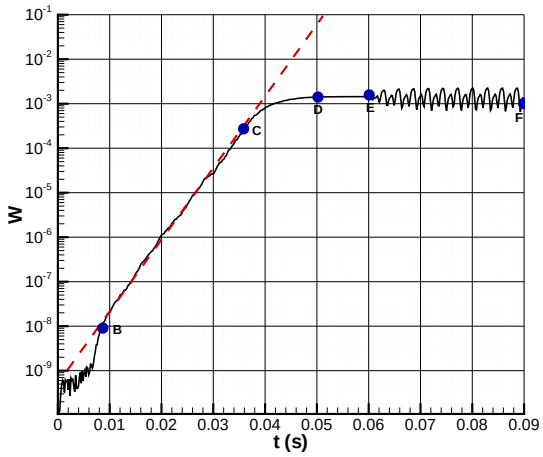

Figure 3. Time evolution of $\mid w \mid$ in logarithmic scale, $L_z = 0.8$, $\theta = 32^o$. Continuous line : numerical simulation, Dashed line : linear amplification rate.

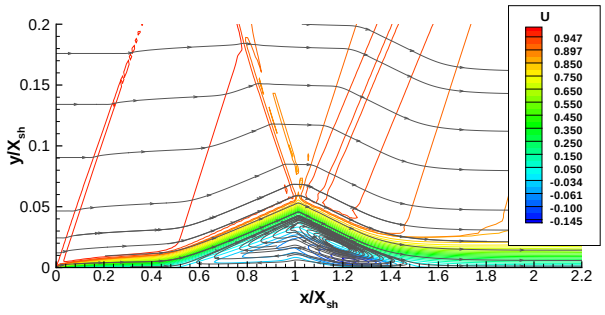

Figure 4. Iso-lines of longitudinal velocity $\overline{U}(x, y)$ and streamlines. $\theta = 32^o$, Re$= 10^5$.

5. Global Instability Analysis

5.1. Small Perturbation Technique

The analysis of flow stability is based on the compressible Navier-Stokes equations. The instantaneous flow is written as the superposition of a basic flow and of a small perturbation. All physical quantities q (velocity, pressure, etc) are thus decomposed into an unperturbed value and a fluctuating one:

$$\mathbf{q}(x, y, z, t) = \overline{\mathbf{Q}}(x, y, z) + \varepsilon\, \mathbf{q}'(x, y, z, t) \tag{1}$$

with $\overline{\mathbf{Q}} = (\overline{U}, \overline{V}, \overline{W}, \overline{P}, \overline{T})^T$ and $\mathbf{q}' = (u', v', w', p', T')^T$ representing the basic flow and the unsteady three-dimensional infinitesimal perturbations, respectively.

5.2. Base Flow Computation

The availability of a two-dimensional basic state $\overline{Q}$ will be known analytically only in exceptional model flows; in the large majority of cases of industrial interest it must be determined by numerical or experimental means. An accurate basic state is a prerequisite for reliability of the instability results obtained; if numerical residuals exist in the basic state (at $\mathcal{O}(1)$) they will act as forcing terms in the $\mathcal{O}(\varepsilon)$ disturbance equations and will result in erroneous instability predictions. In laminar flows, current hardware capabilities permit determining a basic state using 2D DNS at arbitrary high resolution. Thereafter, the basic flow is obtained by the resolution of the two-dimensional equations of motion. Fig. 4 shows the topology of the interaction zone for $\theta = 32^o$. The separated zone extends on $L_s \simeq 1$ and is only one piece (not secondary zone). After to compute the basic flow solutions on computational domain using high resolution grid inaccessible to the instability analysis, a cubic spline interpolation scheme is used to transpose the basic flow solution on to the stability grid. The basic flow solutions are converged in time to within a tolerance $tol \equiv \mid (g_{t_0+\Delta t} - g_{t_0})\,/g_{t_0} \mid < 10^{-10}$, where g is an integral measure of the flow or the value of a local flow quantity.

5.3. Perturbation Form

According to the base flow properties, the perturbation can be sought inhomogeneous in x and y directions and periodic in z and t. When substituting (1) into the governing equations, taking $\varepsilon \ll 1$ and linearizing about $\overline{\mathbf{Q}}$, any fluctuating quantity is written as

$$\mathbf{q}'(x, y, z, t) = \hat{\mathbf{q}}(x, y)\, \exp\left[i\,(\beta z - \omega t)\right] + c.c. \tag{2}$$

with $\hat{\mathbf{q}} = (\hat{u}, \hat{v}, \hat{w}, \hat{p}, \hat{T})^t$ representing the vector of two-dimensional complex amplitude functions of the infinitesimal three-dimensional perturbations. In the present temporal framework, β is taken to be a real wavenumber parameter describing an eigenmode in the z-direction, while the complex eigenvalue ω, and the associated eigenvectors $\hat{\mathbf{q}}$ are sought. The real part of the eigenvalue, Re(ω), is related with the frequency of the global eigenmode while the imaginary part represents its growth/damping rate; a positive value of Im(ω) indicates an exponential growth of the instability mode while Im(ω) < 0 denotes a decay of $\tilde{\mathbf{q}}$ in time.

5.4. THE COMPRESSIBLE BIGLOBAL EIGENVALUE PROBLEM

The linear disturbance equations of BiGlobal stability analysis are obtained at $\mathcal{O}(\varepsilon)$ by substituting the decomposition (1) into the equations of motion, subtracting out the $\mathcal{O}(1)$ basic flow terms and neglecting terms at $\mathcal{O}(\varepsilon^2)$. The system for the determination of the eigenvalue and the associated eigenfunctions $\hat{\mathbf{q}}$ in its most general form can be written as the complex non-symmetric generalized eigenvalue problem

$$\mathcal{L}(\omega; \mathrm{Re}, \beta)\hat{\mathbf{q}}(x, y) = 0 \tag{3}$$

with the linear operator $\mathcal{L}$ written as

$$\mathcal{L} = \mathbf{M}_1\frac{\partial^2}{\partial x^2} + \mathbf{M}_2\frac{\partial^2}{\partial y^2} + \mathbf{M}_3\frac{\partial^2}{\partial x \partial y} + \mathbf{M}_4\frac{\partial}{\partial x} + \mathbf{M}_5\frac{\partial}{\partial y} + \mathbf{M}_6$$

where $\mathbf{M}_j$ are six (5×5) complex matrices which are functions of the base flow and of the coefficients ω and β. The detail of operator $\mathcal{L}$ is presented in reference[5].
The number of boundary conditions depends on the operator order and the nature of the partial derivative system. In the case of a compressible flow, the system is elliptic it is thus necessary to write ten boundary conditions in each direction.
The computational domain used for the stability approach is: $\mathcal{D} = [x_0; x_n] \times [0; y_n] = [280; 400] \times [0; 60]$. Various domains have been used with several values of x_n and y_n in order to test the independence of the solution with respect to this domain as well as the influence of the boundary conditions. The field chosen above represents a good compromise between the independence of the solution with respect to x_n and y_n and the computation cost.
At $x = x_0$, homogeneous Dirichlet boundary conditions applied on all disturbances are used; this choice corresponds to disturbances generated within the examined basic flow field: $\hat{\mathbf{q}} = (\hat{u}, \hat{v}, \hat{w}, \hat{p}, \hat{T})(x_0, y) = 0 \forall y \in [0, y_n]$. At $x = x_n$, quadratic extrapolation of all disturbance quantities, except for the pressure, from the interior of the integration domain is performed. A compatibility relation on the fluctuating pressure gradient is applied at the exit boundary: $\partial\hat{p}/\partial x = \chi(x_n)$. At the solid wall, viscous boundary conditions are imposed on all disturbance velocity components $\hat{u} = \hat{v} = \hat{w} = 0$ and the temperature perturbation is set to zero $\hat{T} = 0$. A compatibility condition is also imposed for the pressure gradient $\partial\hat{p}/\partial y = \chi(0)$ at the wall. Similar boundary conditions are imposed at $y = y_n$.

5.5. NUMERICAL DISCRETIZATION

As the requirements for the computational grid of the LES simulation of the base flow are not identical to those of the global stability computation, it is appropriate to interpolate

the base flow on the stability grid. The principal difficulty is that this interpolation must be sufficiently accurate so that the interpolation does not modify "too much" the results of the stability computation on this interpolated base flow. The interpolation is carried out by the bi-cubic spline (NAG library) which guarantees a weak interpolation error.
Numerical methods of high formal order of accuracy are necessary since the coupled spatial discretization in the numerical solution of the eigenvalue problem (3) cannot be increased at will in order to achieve convergence; In the present analysis spectral collocation has been used, based on the Chebychev Gauss-Lobatto (CGL) points for each direction x and y. Because of the complexity of the basic flow (shock wave, separated boundary layer, etc.), a single-domain algorithm cannot be used to accurately describe the entire domain of the flow. In order to extend the BiGlobal stability analysis methodology to complex geometries with a certain degree of regularity, the spectral multi-domain algorithm is an obvious candidate. The Chebyshev intervals $(\zeta, \xi) = [-1; +1]^2$ are transformed to the computational domain $\mathcal{D}$ by use of the following mapping. In normal y-direction, a mapping transformation for semi-infinite domains of boundary-layer type is used

$$y = \frac{a_0(1-\xi)}{a_1+\xi}, \text{ with } a_0 = \frac{y_a y_n}{y_n - 2y_a} \text{ and } a_1 = 1 + 2\frac{a_0}{y_n},$$

y_n is the upper boundary domain and $y_a \sim \delta_0(X^\star = 1)$ is the coordinate such as in $[0; y_a]$ there are fifty percent of the total number of points. In streamwise x-direction a spectral multi-domain method is used

$$\begin{aligned}
&x \in [x_0; x_d], \quad x = x_0 + \frac{(x_a - x_0)(x_d - x_0)(1+\zeta)}{(x_d + x_0 - 2x_a)\left(1 + \frac{2(x_a - x_0)}{(x_d + x_0 - 2x_a)} - \zeta\right)}, \\
&x \in [x_d; x_r], \quad x = x_i + x_d \frac{\tan\left(\frac{c\pi}{2}\zeta\right)}{\tan\left(\frac{c\pi}{2}\right)}, \ c = 0.9, \\
&x \in [x_r; x_n], \quad x = x_r + \frac{(x_b - x_r)(x_n - x_r)(1+\zeta)}{(x_n + x_r - 2x_b)\left(1 + \frac{2(x_b - x_r)}{(x_n + x_r - 2x_b)} - \zeta\right)}.
\end{aligned}$$

where x_d, x_i and x_r correspond respectively to the separation, interaction and reattachment points of the basic flow. At the interface of the domains, continuity and derivability of the disturbances are imposed.
Using the tools presented, the compressible BiGlobal linear eigenvalue problem (3) is transformed into a discrete matrix eigenvalue problem:

$$\left[\mathcal{A}(\mathrm{Re}, \beta) - \omega \mathcal{B}(\mathrm{Re}, \beta)\right] \hat{\mathbf{Z}} = 0, \tag{4}$$

where $\hat{\mathbf{Z}} = \{\hat{\mathbf{q}}_{ij}\}$. A standard eigenvalue subroutine may now be used to compute the eigenvalues. The first method to solve this algebraic system (4) is the QZ algorithm in the absence of prior information on interesting regions of the parameter space. When the interesting zone of the spectrum is identified, a less expensive algorithm, the Arnoldi algorithm[4], is used to compute a part only of the spectrum as well as the associated eigenfunctions.

6. Global linear stability results

The approach described in the preceding sections is employed to compute linear global stability for various values of the incident shock wave angle from $\theta = 31^o$ to $\theta = 33^o$. Certain characteristics observed in the DNS are found. The critical shock angle beyond which the flow becomes unstable is very close: $\theta_c = 31.8^o$ for the stability analysis and

	DNS	**STABILITY**
Temporal amplification rate	3.71×10^{-4}	3.85×10^{-4}
Wave length $\lambda = 2\pi/\beta$	0.8 ± 2	0.798
Critical incident shock angle θ_c	31^o7	31^o8

Table 3. Comparison between DNS and global stability analysis.

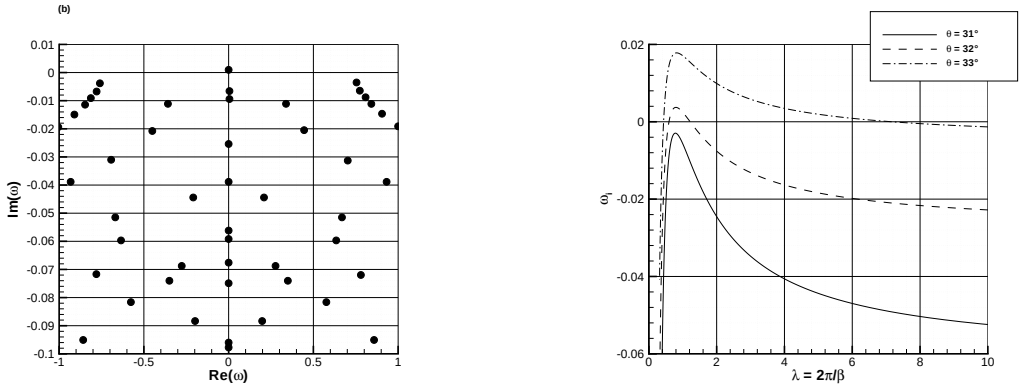

Figure 5. Left: Discretized linear stability spectrum: $\theta = 32^o$, $\beta = 7.86$. Right: Temporal growth rate $\mathrm{Im}(\omega)$ versus spanwise wavelength $\lambda = 2\pi/\beta$ for various incident shock angle θ.

$\theta_c = 31.7^o$ for the DNS. The eigenvalue spectra in the neighbourhood of $\omega = 0$ and for $\theta = 32^o$ is shown in figure 5-(a). At this set of parameters (Re, M and θ), the most unstable mode is a three-dimensional stationary perturbation. The most unstable wavelength for example for $\theta = 32^o$ is equal to 0.7987, which is very close to that observed in the DNS which is rather around 0.8. The evolution of the amplification rate, $\mathrm{Im}(\omega)$, according to the wavelength λ for various θ values is presented on figure 5-(b). Table 3 gives some comparative data between the direct numerical simulation and the analysis of stability. Fig. 6 presents a comparison between the eigenfunction of the most unstable mode resulting from the analysis of stability and the disturbance, in the linear regime, extracted from the DNS. Most of the activity in all disturbance eigenfunctions is confined within the boundary layer and to some degree in the vicinity of the reflected shock. The upstream zone of SWTBLI is innocuous in agreement with DNS results. The neighbourhood of the basic laminar flow separation point is weakly affected, as is clearly demonstrated by the level of activity of all disturbance velocity components and pressure in that region.

7. Conclusions

Main objective of this paper was to highlight that an interaction between an oblique shock wave impacting a laminar boundary layer developing on a flat plate could be the generating seat of a global instability of low frequency self-sustained oscillations. Therefore, three-dimensional direct numerical simulations were carried out for a configuration close to that of [2] where the incident shock angle is gradually increased.
These numerical simulations highlighted a complex process in the onset of unsteady dynamics when the angle of the incident shock increases. These numerical computations

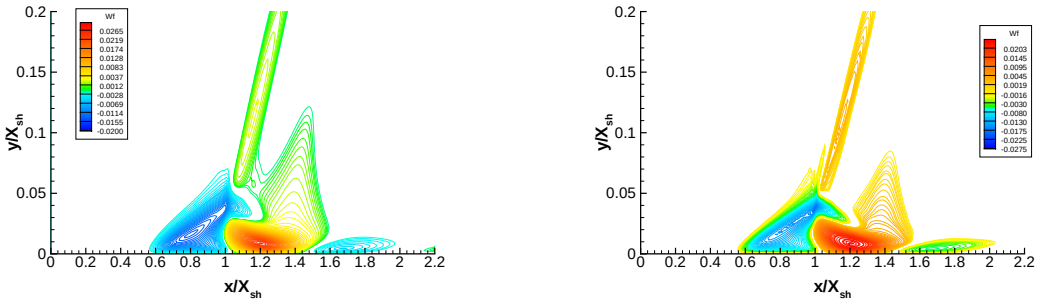

Figure 6. Left: normalized disturbance spanwise velocity for the most unstable global mode. Right: perturbed spanwise velocity from the DNS in (x, y)-plan for $t = 0.025$ at $z = 0.4$.

have shown that before becoming unsteady, the SWBLI goes through a phase where the flow becomes three-dimensional and stationary (for $\theta > 31.7^o$). However, this state is unstable and can lead to a fully three-dimensional and unsteady flow. The final state is reached more quickly when the angle of the incident shock is large.
When the spanwise dimension L_z is large enough, the main spanwise wavelength of the disturbance is close to $\lambda_z = 0.8$. In the interaction, the topology of the separated zone is complex and mainly characterized by cells in the spanwise direction where the flow is alternatively separated and reattached. This topologically complex zone exhibits an unsteady self-sustained low frequency dynamics close to 700 Hz. For more details, see [1, 5].
Linearized global stability analysis was carried out in order to find the physical origin of the bifurcation generating the three-dimensional character of the flow. This analysis highlighted that beyond a critical angle of the incident shock wave the flow becomes linearly globally unstable, a stationary three-dimensional mode with characteristics very close to those highlighted in the direct numerical simulation has been observed. The wavelength, the temporal amplification rate as well as the main space characteristics of the disturbance is found.

Acknowledgements

Computing time was provided by Institut du Développement et des Ressources en Informatique Scientifique (IDRIS)-CNRS.

References

[1] J.P. Boin, J.-Ch. Robinet, Ch. Corre, and H. Deniau. 3D steady and unsteady bifurcations in a shock-wave / laminar boundary layer interaction; a numerical study. *Theoret. Comput. Fluid Dynamics*, 20(3):163–180, 2006.

[2] G. Degrez, C.H. Boccadoro, and J.F. Wendt. The interaction of an oblique shock wave with a laminar boundary layer revisited. an experimental and numerical study. *J. Fluid. Mech.*, 177:247–263, 1987.

[3] M.S. Liou and J. Edwards. Low-diffusion flux-splitting methods for flows at all speeds. *AIAA Journal*, 36:1610–1617, 1998.

[4] C. Yang R. B. Lehoucq, D. C. Sorensen. Arpack user's guide: Solution of large scale eigenvalue problems with implicitly restarted arnoldi methods. Technical Note, 1997.

[5] J.-Ch. Robinet. Bifurcations in shock wave / laminar boundary layer interaction: Global instability approach. *J. Fluid Mech.*, 578:67–94, 2007.